

Available online at www.sciencedirect.com



ultramicroscopy

Ultramicroscopy 106 (2006) 423-431

www.elsevier.com/locate/ultramic

Quantitative Fresnel Lorentz microscopy and the transport of intensity equation

S. McVitie*, M. Cushley

Department of Physics and Astronomy, University of Glasgow, Glasgow, Gl2 8QQ, UK

Received 7 September 2005; received in revised form 1 December 2005; accepted 1 December 2005

Abstract

Imaging of the magnetic structure of thin films by the Fresnel mode of Lorentz microscopy has been re-evaluated in terms of the Ampérian current density within a sample. The conditions for which this imaging can be treated as linear are discussed for quantitative application. Additionally, the consequences for magnetic phase reconstruction using the transport of intensity equation for defocused images are considered. While the range of applicability may initially appear rather limited examples of objects containing different spatial frequency components are used to illustrate the possibilities where relatively large defocus values may be used.

© 2005 Elsevier B.V. All rights reserved.

Keywords: Transmission electron microscopy; Lorentz microscopy; Transport of intensity equation; Magnetic thin films; Magnetic domains; Magnetic domain walls

1. Introduction

Imaging of magnetic domain walls has been one of the main features of the Fresnel mode of Lorentz microscopy in the transmission electron microscope (TEM) since its inception [1]. A number of authors have used this technique to infer the domain wall width from images taken at different values of defocus with good agreement between experiment and theory [2,3]. More recently the transport of intensity equation (TIE) [4] has been developed to allow Fresnel images to quantitatively reconstruct the phase associated with magnetic thin films [5,6]. While Fresnel imaging of domain walls is generally considered to be a non-linear imaging mode, the TIE method offers the possibility that, under certain conditions, the information in the images can be linearly interpreted and so used directly in a quantitative manner.

In this paper, we address the linear aspects of Fresnel imaging for magnetic thin films and relate this to the TIE results that have recently been published. In Section 2 we show that, under suitable conditions, the Fresnel image intensity of a magnetic material may be interpreted linearly

in terms of the Ampérian current density component parallel to the electron beam. However, while it can be proven that Fresnel images can be used successfully to reproduce, for example, domain wall profiles caution must be exercised when presenting such data. In Section 3 model calculations are presented from some simple 1-D wall structures to illustrate the power of the technique and establish useful operating conditions. The consequences for TIE reconstruction of magnetic films are then presented in Section 4, with conclusions and future prospects for this type of imaging considered in Section 5.

2. Quantitative magnetic Fresnel imaging

Understanding the contrast mechanisms in Fresnel imaging is well established in the TEM [7–9]. Mostly this has been applied to pure phase objects with particular emphasis on weak phase objects. Generally, magnetic thin films may not be regarded as weak phase objects. However, the recent applications of the TIE formulation, which utilises Fresnel images, has opened up the possibility of a more general phase imaging technique. In principle it offers a non-holographic reconstruction of the object phase. In this section, the wave-optical origin of Fresnel contrast is

^{*}Corresponding author. Tel.: +44 141 330 6895; fax: +44 141 330 4464. *E-mail address:* s.mcvitie@physics.gla.ac.uk (S. McVitie).

considered for magnetic materials and the range of applicability of the linear regime of imaging addressed.

The wave optical derivation of the Fresnel image intensity has been tackled by a number of authors [6,7,10,11]. For simplicity, we consider an object exhibiting only phase variation with unit amplitude everywhere. We write the phase function as $\phi(\mathbf{r})$, noting that the phase is a 2-D function for the in-plane spatial coordinates of the sample \mathbf{r} given as (x,y). The electron wave (travelling in the z direction) is taken as uniform prior to the sample. Following the derivations in the references quoted we can derive the result, essentially Eq. (3) in Ref. [6], for the intensity in the Fresnel image as

$$I(\mathbf{r}, \Delta) = 1 - \frac{\Delta \lambda}{2\pi} \nabla_{\perp}^{2} [\phi(\mathbf{r})]$$
 (1)

with λ the electron wavelength, Δ the defocus distance and ∇_{\perp} the Laplacian relating to in-plane coordinates only. The derivation assumes that higher order terms in defocus are neglected. In effect the validity of this approach also depends on the small angle approximation applied to the contrast transfer function which we write as a 2-D reciprocal space function in Fourier space (k space). The approximation is valid for $\Delta \lambda k^2 \ll 1$. Therefore the image, under these constraints, gives us linear information on the in-plane Laplacian of the phase of the object function. While the above equation is true for general phase objects we now turn our attention specifically to magnetic contributions to the phase. We return to the validity of the approximation later.

We now consider the magnetic phase contribution to gain an insight into the relationship between an object's magnetisation and its phase [12]. This will allow us to interpret Eq. (1), i.e. the Fresnel image intensity, in terms of the sample magnetisation. The phase associated with a magnetic object can be written using the Aharonov–Bohm effect [13] in terms of the magnetic vector potential (A). The argument given in Ref. [12] is reproduced briefly here to put in to the context of quantification of Fresnel imaging, the phase is written as an integral along the electron path:

$$\phi(\mathbf{r}) = -\frac{e}{\hbar} \int_{-\infty}^{\infty} \mathbf{A} \cdot \mathbf{dl}$$
 (2)

with e the electronic charge and \hbar is Planck's constant divided by 2π . Now it would be useful to relate the phase to the magnetisation and we proceed to show how this can be achieved. Firstly, it is necessary to write down the form of the magnetic vector potential. This can be found in most textbooks on electromagnetism and we write here as a 3-D function

$$\mathbf{A}(\mathbf{r}) = \frac{1}{4\pi} \iiint \frac{\nabla \times \mathbf{B}(\mathbf{r}')}{|\mathbf{r} - \mathbf{r}'|} \, \mathbf{d}^3 \mathbf{r}' \tag{3}$$

with the integration over all sources having finite curl of magnetic induction \mathbf{B} ($\nabla \times \mathbf{B}(\mathbf{r}')$). Note in this case the position vectors are in three dimensions. Further simplifi-

cation is achieved by noting that this function is a convolution of $\nabla \times \mathbf{B}(\mathbf{r})$ and the geometric function $1/4\pi r$ with $r = |\mathbf{r}|$. Furthermore, if we were to write this in reciprocal space, i.e. the Fourier transform of $\mathbf{A}(\mathbf{r})$, we see that

$$\mathbf{A}(\mathbf{k}) = \frac{1}{4\pi \mathbf{k}^2} FT[\nabla \times \mathbf{B}(\mathbf{r})]. \tag{4}$$

Note particularly the $1/\mathbf{k}^2$ term, makes magnetic Fresnel image interpretation quite simple, as seen later. However, it is important to understand that it is useful to think of the magnetic vector potential in terms of the curl of the magnetic induction. (This argument is effectively the same as viewing the magnetic scalar potential written as a convolution of the divergence of the magnetisation and the function $1/4\pi r$ [14]).

The relevant quantity, $\nabla \times \mathbf{B}(\mathbf{r})$, is just one of Maxwell's equations of electromagnetism and can be written in terms of current densities with terms for conduction, Ampérian and displacement currents. For a general description we can retain all these terms so that $\nabla \times \mathbf{B}(\mathbf{r}) = \mu_o \mathbf{J}(\mathbf{r})$, with μ_o the permeability of free space, in which all the current density $(\mathbf{J}(\mathbf{r}))$ contributions are included. In many cases in the TEM we deal with a static situation (i.e. no displacement currents) and there are no conduction currents present. In such cases the curl of magnetic induction and magnetisation are the same except for the multiplicative μ_o term. Therefore we can now identify the Ampérian current density as the important term and this is simply $\nabla \times \mathbf{M}(\mathbf{r})$.

Going back to the equation for the phase we can now write this to include the Ampérian current density as

$$\phi(\mathbf{r}) = -\frac{e\mu_0}{4\pi\hbar r} \otimes \int_{-\infty}^{\infty} (\nabla \times \mathbf{M}(\mathbf{r})) \cdot \mathbf{dl}$$
 (5)

with the symbol \otimes denoting a convolution in 2-D here. It should be noted that we now have the local quantity associated with the magnetisation in the sample that results in contrast in the Fresnel image, namely the integral of the Ampérian current density component along the electron path. In the simplest case the thin film plane is normal to the electron beam (z direction) with no variation of magnetisation through the film thickness (t). Therefore the integral part of (5) becomes $((\nabla \times \mathbf{M}(\mathbf{r})).\hat{\mathbf{z}})t$ in this instance. We can now see that the out-of-plane component of Ampérian current density is responsible for the contrast in Lorentz Fresnel imaging. In general it is the component parallel to the electron path.

Putting this into the equation for the image intensity Eq. (1) we see, at first, what appears to be a rather complex function. At this point we note that in reciprocal space the Laplacian of a function is proportional to \mathbf{k}^2 and that the Fourier transform of the $1/4\pi r$ term is proportional to $1/\mathbf{k}^2$ [15,16]. In combining this information, i.e. taking the Fourier transform of Eq. (1), substituting the transformed phase and then taking the inverse transform, we are

left with

$$I(\mathbf{r}, \Delta) = 1 - \Delta \frac{e\mu_{o}\lambda t}{h} (\nabla \times \mathbf{M}(\mathbf{r})).\hat{\mathbf{z}}$$
 (6)

which is the intensity of a Fresnel image at small defocus Δ for a thin film normal to the beam with no magnetisation variation through the thickness. Note that the denominator contains just Planck's constant, h, rather than \hbar . For the case of variable magnetisation and the beam not normal to the film plane the curl of the magnetisation term will be an integral through the thickness of the projected film. We return to the specifics of magnetisation curl distributions in the next section, with examples from domain walls being analysed.

We return to the issue of the range of defocus values under which the assumptions leading to Eq. (6) being valid apply. This is of particular importance if Fresnel images are to be treated in a quantitative manner. Furthermore this is very relevant to the range of validity of the TIE equation. The assumption regarding the small defocus range centred on rewriting the contrast transfer function [6] in the limit of the small angle approximation i.e. $\Delta \lambda \mathbf{k}^2 \ll 1$ which has also been discussed by other authors [10,11]. The spatial frequencies in the image determine the extent with which we can apply this equation for a given defocus. This can be illustrated simply by looking at the contrast transfer function for this situation $T(\mathbf{k}) = \sin(\pi \lambda \Delta \mathbf{k}^2)$. (Note we have omitted the factor 2 that normally multiplies this function). An example of a transfer function for a system dominated by the defocus term is shown in Fig. 1. Here the defocus has been chosen to be 20 µm and the transfer function is shown by the solid line. For comparison the function $T'(\mathbf{k}) = \pi \lambda \Delta \mathbf{k}^2$ i.e. the small angle approximation is shown by the lighter coloured line and it is apparent that the two lines start to deviate at spatial frequencies above 0.05 nm⁻¹. The condition for small defocus is the region below which the curves are effectively identical. Also of note is the first point at which the transfer function crosses the axis $(\Delta \lambda \mathbf{k}^2 = 1)$. Up to the latter point all the spatial frequency information is transferred with the same sign.

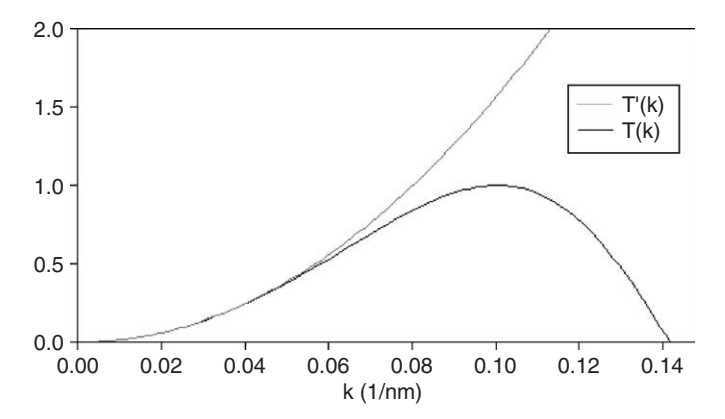


Fig. 1. Curves showing the TEM transfer functions $T(\mathbf{k})$ and $T'(\mathbf{k})$ for small \mathbf{k} values with a defocus of $20\,\mu\mathrm{m}$. Both the departure from the linear regime and the first zero of the transfer function can be observed.

Table 1 Illustration of characteristic resolution for transfer function due to defocus for linear regime and the location of the first zero

<u>Δ (μm)</u>	Linear d(nm)	1st zero d(nm)
2	7.1	2.2
5	11.2	3.5
10	15.8	5.0
20	22.4	7.1
50	35.4	11.2
100	50.0	15.8
200	70.7	22.4
500	111.8	35.4
1000	158.1	50.0

The calculated values are from the spatial frequencies at which these points are located for 200 kV electrons.

From these two conditions it is possible to assign a resolution (d) of spatial frequency information using $|\mathbf{k}| = 1/d$ and this is shown in Table 1 for 200 kV electrons. In the case of the linear imaging condition we have used the limit $\Delta \lambda \mathbf{k}^2 = 0.1$ to maintain linear behaviour consistent with Fig. 1. It is apparent that the resolution for the linear region limit is poorer than that defined by the first zero of the transfer function. To be able to assess the meaning and possible validity of these figures it is necessary to look at some examples and determine the practical regime of use for a given defocus and the signal levels involved.

3. Results from simulated images

Eq. (6) reveals that image intensity can be calculated easily from knowledge of the microscope parameters and the out of plane component of magnetisation curl when the linear imaging conditions are applicable. However it, would be instructive to calculate the images using the correct aberration function for any defocus and then compare the expected results with the linear regime given by Eq. (6). Once an object's magnetisation distribution has been defined, calculation of the phase can be made from Eq. (5) or by using an algorithm based on Fourier series representation of the magnetisation [17] which we have incorporated into our image processing software [18]. The exit wave and the effect of aberrations are then calculated as from standard wave optical treatment [7,8]. The image wave is then calculated by an inverse Fourier transform of the aberrated wave and then multiplied by its complex conjugate to give the intensity. We used microscope parameters based on a Lorentz lens in a FEI Tecnai TEM operating at 200 kV with $C_s = 8000 \,\mathrm{mm}$ and $\lambda = 2.51 \text{ pm}.$

The process described above can be calculated for any magnetisation distribution in a thin film and we have used it for images simulated from micromagnetic packages freely available in the public domain such as such as Object Oriented Micromagnetic Framework (OOMMF) [19]. However, to illustrate the use of the calculations detailed in this paper we have decided to concentrate on simple 1-D

wall models. While 1-D wall models can have a long range and detailed structure e.g. see Ref. [20], we have chosen three simple models of 180° walls in thin films namely: (i) linear, (ii) hyperbolic tangent and (iii) arctangent. The wall models were respectively (i) $M_{\nu}(x) = M_{\rm s}x/\delta$ (for $-\delta < x < \delta$), (ii) $M_v(x) = M_s \tanh(x/\delta)$ and (iii) $M_v(x) =$ M_s arctan (x/δ) , with M_s the saturation magnetisation and δ the width parameter. These are chosen to illustrate the viability of the method and give an indication of how the detail of the wall structure is imaged. Furthermore as these are 1-D walls, being a function of x only, we do not need to bother with any x or z component of magnetisation as these give no out of plane curl component for infinitely long walls. For the wall width we use the definition of the FWHM of $\partial M_{\nu}(x)/\partial x$ which gives a width of 2δ for (i) and (iii) and 1.76δ for (ii). This definition is used as the Fresnel image, under linear imaging conditions, for these 1-D walls is the derivative of the y-component of magnetisation from a simple consideration of Eq. (6). In each case a 2-D image was created with a pair of parallel walls to ensure that the phase was periodic. Each image comprised 1024 × 1024 pixels with 1 nm pixel spacing. Calculations were also performed with larger pixel spacing but the results did not show appreciable changes for the systems studied here. If we consider a pixel spacing p the largest spatial frequency present in such an image is $|\mathbf{k}| = 1/(2p)$. We can substitute this spatial frequency into the two conditions defined at the end of the last section defining the limit of the imaging conditions and calculate an associated defocus. For the linear limit we find $\Delta = 0.1(2p)^2/\lambda = 0.16 \,\mu\text{m}$ and for no reversal of the transfer function $\Delta = (2p)^2/\lambda = 1.6 \,\mu\text{m}$. As we shall see these figures indicate very small values of defocus for observation of magnetic contrast under linear imaging conditions. However, for many magnetic studies there is little information at the highest spatial frequency and therefore it is possible that higher defocus values can be used.

An example of each type of wall profile from the calculated $\nabla \times \mathbf{M}$ component is shown in Fig. 2 for $\delta = 20\,\mathrm{nm}$ across a single wall in each case. The curl of the magnetisation was calculated using fast Fourier transforms. It is apparent that the smooth variations of the arctangent and hyperbolic tangent have a form similar to that measured from previous studies of domain walls in thin films [3,18]. The linear wall on the other hand has a top hat shape which is useful in that changes to this shape are much more visually apparent with defocus. Obviously, the linear wall has more significant high spatial frequency components compared to the other two walls.

The parameter range chosen for study had values of the domain wall width parameter of $\delta=1,5,10,20,40\,\mathrm{nm}$. This ranged from very narrow walls to wall widths expected in 20-nm-thick films of soft materials. The material parameters chosen for the image calculation corresponded to permalloy (Ni₈₀Fe₂₀) of thickness 20 nm which has saturation magnetisation corresponding to $\mu_{\rm o}M_{\rm s}=1.0\,\mathrm{T}$. However, the results for imaging intensity

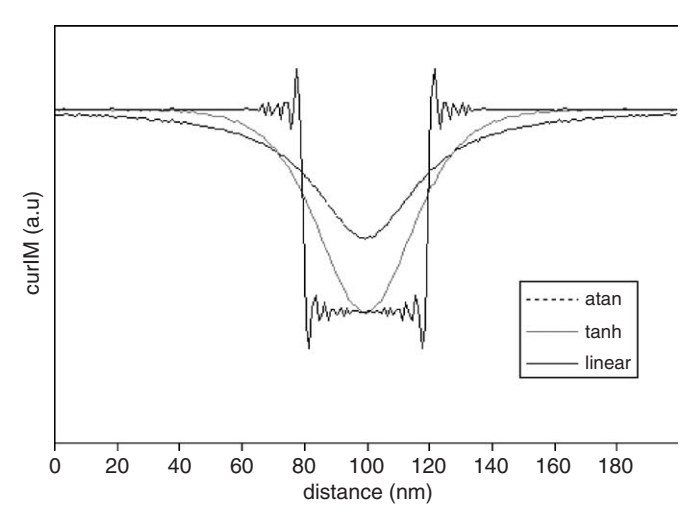


Fig. 2. Spatial variation of out of plane component of $\nabla \times \mathbf{M}$ across a domain wall for the three wall models described in the text each having a domain wall width parameter $\delta = 20 \, \mathrm{nm}$.

can be scaled with both thickness and magnetisation as can be seen from Eq. (6). The defocus values chosen for the images were $\Delta=2,20,50,100,200$ and $500\,\mu m$ which was expected to cover both the linear and non-linear images ranges for most of the walls. Calculations were performed using the commercial package Digital Micrograph available from Gatan Inc. We present results from divergent walls (black lines on Fresnel images) for consistency with earlier work [2]; however, within each image data was also available for the convergent wall i.e. the other wall of the pair. It was found that the data for both types of wall were identical within the linear regime with noticeable differences outside of this range. We can see this effect more clearly when we discuss the TIE formulation in the next section.

Assessment of the images taken at different defocus were determined by the relative contrast level between the depth of the divergent wall image and the background far away from the wall i.e. the visibility [2]. Additionally, we also measured the width of the wall determined from the FWHM of the divergent wall image from the base level. In the case of the wall visibility the value expected from the linear imaging conditions is effectively the second term in Eq. (6) which should increase linearly with defocus. The width of the intensity profile should not change in the linear regime and should be given by the value of 1.76 or 2.0δ for the walls considered i.e. the wall width of the magnetisation profile. However, outside of the linear range this is expected to vary considerably.

Image calculations for the different walls showed very similar behaviour; however, as expected the values of defocus at which deviations from the linear approximation were observed varied with the wall width parameter. This is consistent as the resolution required varied with the spatial frequencies contained within the object. The wall visibility is shown in Fig. 3 for three of the arctangent walls. The points indicate the measurements from the correctly

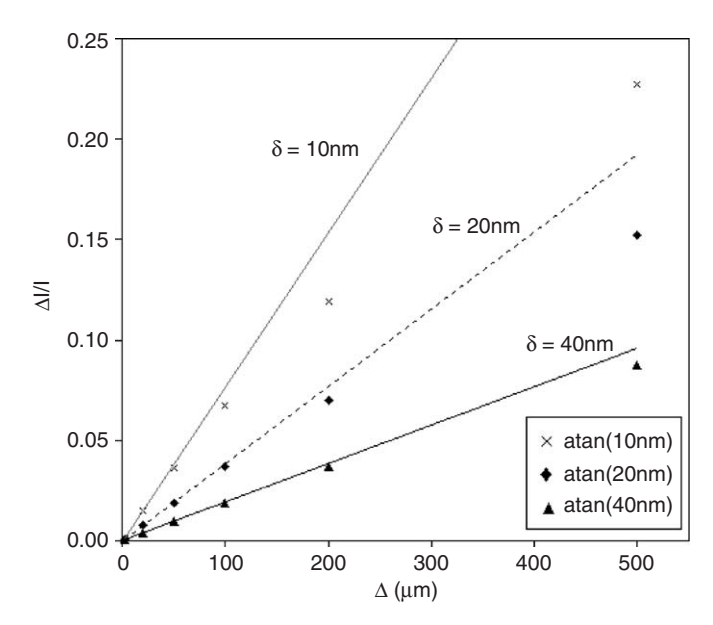


Fig. 3. Variation of visibility $(\Delta I/I)$ of divergent domain wall as a function of defocus for three arctangent walls with width parameters as indicated. The points are from calculation of the simulated Fresnel images. The lines represent predicted values for the linear imaging conditions as assumed from Eq. (7) and plotted over the whole defocus range.

calculated Fresnel images, whilst the lines are calculated from what would be expected if the linear regime were applicable over the whole defocus range. In the case of this type of wall the linear relationship can easily be calculated and is found to be

$$\frac{\Delta I}{I} = \frac{2\Delta \lambda e \mu_0 M_s t}{\pi \delta h}.$$
 (7)

The equation predicts the highest contrast for the smallest width wall. For the walls given in Fig. 3 it is clear that the deviation from the linear regime varies markedly with the wall width. The larger the wall width the greater range of defocus in which the measured visibility remains close to the linear predictions. This is true for all the types of wall simulated.

Another check against the linear imaging conditions is to look at the wall width measurements from the images as a function of defocus. These are shown in Fig. 4 for the range of wall widths for the arctangent model. Again these results are representative for all the wall models used. Here, we would expect that within the linear range of imaging the measured wall width would be constant whereas the width should increase with defocus outside of this range. In the case of the latter a linear increase is predicted from classical optics for divergent walls [2]. From the data plotted in Fig. 4 it can be seen that for the wider walls ($\delta = 20$ and 40 nm) the walls have a reasonably constant width up to about $100-200~\mu m$ defocus.

From both the visibility and wall width data it becomes possible to estimate the region in which the linear region is applicable and use the data from Table 1 to give an indication of the resolution of the imaging mode. It is apparent that the transition from the linear region is rather

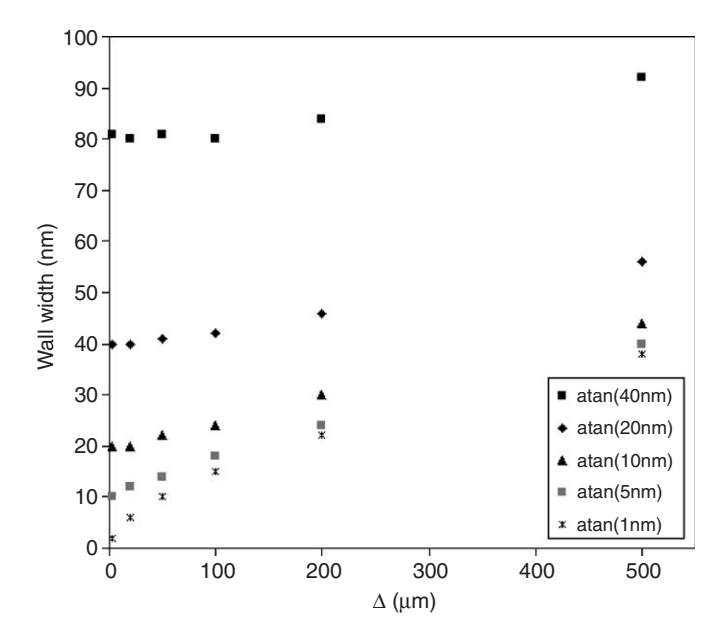


Fig. 4. Plot of divergent domain wall width from Fresnel image simulations for arctangent wall models with different width parameters as indicated. The defined width of the wall from the magnetisation profile is 2δ .

Table 2 Calculated values of optimum defocus for Fresnel imaging of domain walls with a wall width of 2δ for 200 kV electrons

2δ (nm)	Linear Δ (μm)	1st zero Δ (μm)
2	0.1	0.4
10	3.2	10
20	12.7	40
40	50.9	160
40 80	203.7	640

The calculated values of defocus assume a spatial frequency of 2δ for the linear and first zero limits of the transfer function.

gradual and it is possible to still obtain meaningful data outside the condition given by the linear resolution value in Table 1. As a reference Table 2 gives the defocus limit for the linear region and at the first zero of the transfer function is shown for a "resolution" corresponding to the width of the domain wall for each of the walls considered. It is clear that the defocus values given here are much larger than those associated with the maximum possible spatial frequencies in the image calculated earlier from the pixel spacing.

While the arguments presented above give a good indication of the validity of the technique for the dimensions of the magnetic structures simulated, we can look in more detail at the simulated profiles to visually inspect the variation of the wall structures through a range of defocus values. This is shown in Figs. 5 and 6 for linear and arctangent walls, respectively, with width parameter $\delta=20\,\mathrm{nm}$. The walls have been scaled to the peak intensity variation at the smallest defocus assuming a linear increase with focus. Therefore the highest focus values have smaller

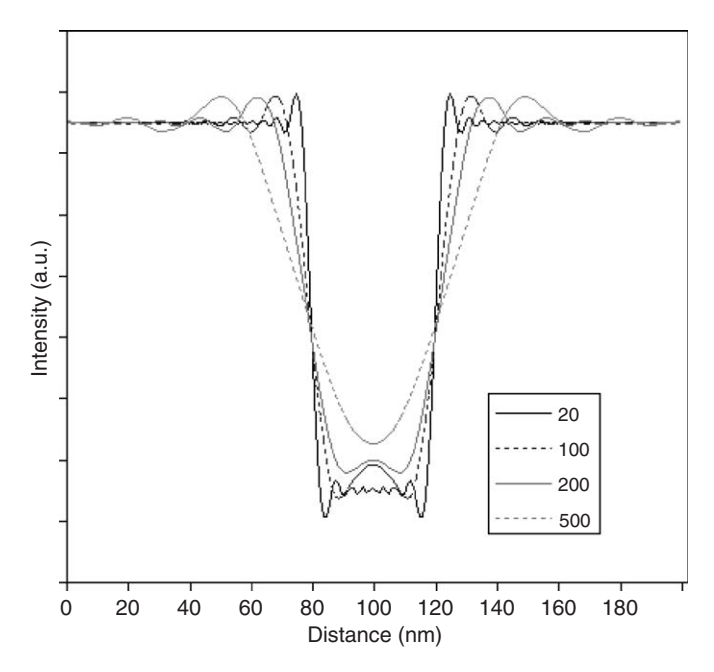


Fig. 5. Intensity variations from Fresnel images of divergent walls for linear wall model ($\delta=20\,\mathrm{nm}$) as a function of defocus given in $\mu\mathrm{m}$ in the legend. The intensity linetraces have been scaled to the $20\,\mu\mathrm{m}$ defocus trace based on linear scaling according to Eq. (6). Note the fall in peak intensity and relative increase in FWHM of the wall with increasing defocus, particularly at the larger defocus values.

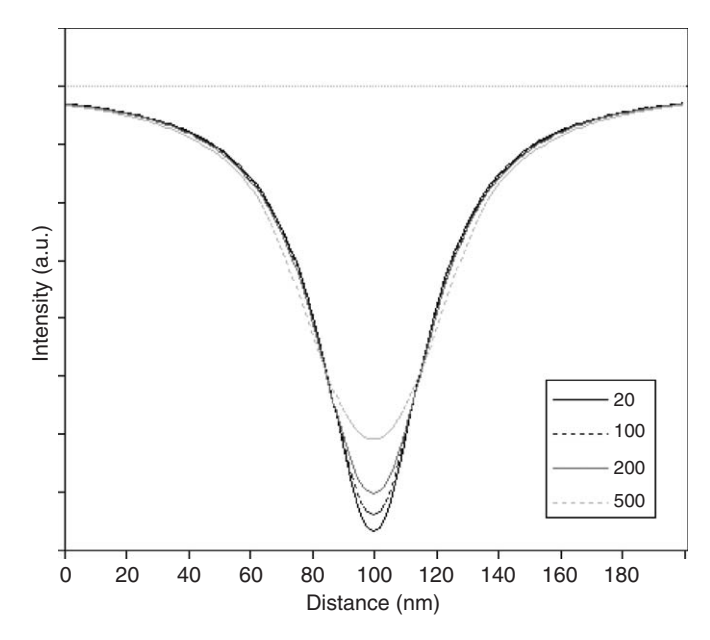


Fig. 6. As Fig. 5 but for the arctangent wall ($\delta = 20 \, \mathrm{nm}$) model. Note that the change is the shape of the smooth arctangent wall is less pronounced than the linear wall than the as defocus is increased.

peaks consistent with the data shown in Fig. 3. The variation in wall shape with defocus is much more pronounced for the linear wall than the arctangent wall. This is not too surprising as the step like nature of the curl of the magnetisation for the linear wall results in greater high spatial frequency components. However, the wall does

maintain a reasonably sound profile up to 200 µm defocus although the edges are beginning to show considerable rounding. In the case of the arctangent wall the profile shape is rather less sensitive to defocus although broadening and reduction in the peak amplitude is clearly visible at 500 µm defocus. For this wall which has a width of 40 nm it is clear that for the figures given in Table 2 the defocus value for the first zero (160 µm) will still give a reasonable profile even though higher spatial frequency components have been suppressed, being outside the linear range. Of course it would be preferable to use the smaller defocus at the limit of the linear range (50 um), however. the visibility of the wall is considerably reduced in this case as can be seen from Fig. 3. One must remember that the "resolution" associated with the wall width here means that we expect some degradation of the signal compared to the $\nabla \times \mathbf{M}$ profile as there are higher spatial frequency contributions to the profile above this resolution. We can see this by comparing Fig. 2 and Figs. 5 and 6, though it is much more apparent in Fig. 5.

4. Relevance to transport of intensity equation

We note that the validity of quantitative Fresnel imaging discussed here applies equally to magnetic phase reconstruction using the TIE method [4]. While the phase functions tend to be rather smooth and slowly varying functions, taking the derivate gives induction component profiles whilst the Laplacian gives the magnetisation curl component discussed above. In TIE the normal procedure is to take three Fresnel images: one in-focus and two equally over and under focus. The useful phase information is contained in the difference between the out of focus images. Hence the visibility signal associated with the walls given in Fig. 3 will be doubled in the difference image for a given defocus. However, this has to be offset with considerations of image registration and alignment required in the TIE method.

Using TIE is becoming an increasingly common method for studying the magnetic structure of thin films [5,10,15,21]. When making comparisons between experimental data and simulations we have to take care in how the results are presented. Lorentz Fresnel images show the curl of the magnetisation in the linear imaging regime which is effectively the second derivative of the magnetic phase. The smoothly varying phase will certainly compare more favourably to the original profile even at the larger defocus and we now show how comparisons fare for the domain walls considered in the previous section.

We can show how this manifests itself by giving results from TIE phase reconstructions from calculated images. Details of the reconstruction can be found in a number of papers [4,6]. As an example we look at the linear wall having wall width of 40 nm ($\delta = 20$ nm). Fig. 7 shows the input phase and the TIE reconstructed phase for defocus values of 20 and 500 μ m across a linear domain wall. Although the latter definitely has a larger deviation from

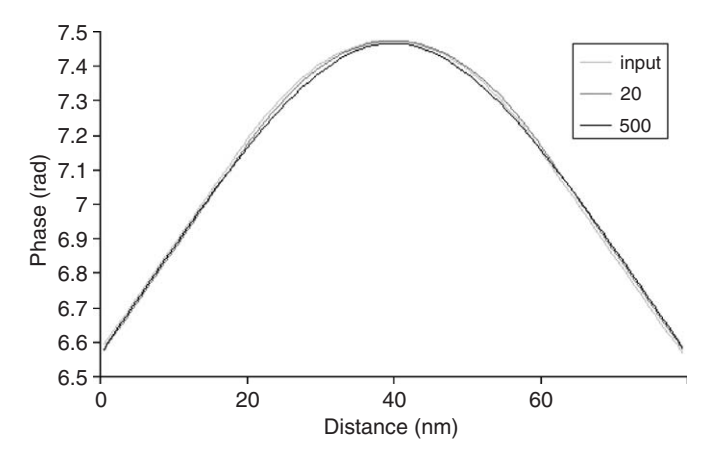


Fig. 7. Phase variation across a linear domain wall ($\delta=20$ nm). The input phase for image calculation is shown together with the reconstructed phase from the TIE for defocus values of 20 and 500 μ m.

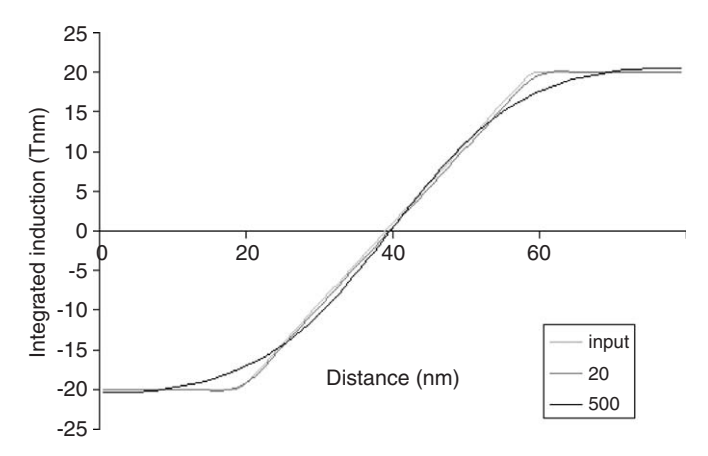


Fig. 8. Induction profile across the domain wall described in Fig. 7. Profiles shown are that calculated from the input phase and from the reconstructed phases at the defocus values of 20 and $500 \, \mu m$.

the input phase, it is very apparent that the phase, which varies smoothly across the domain wall, does not appear to change markedly with defocus from the TIE reconstruction. Compare this with the variation seen in the traces across the wall in Fig. 5 from the Fresnel images at the same defocus values. Taking the derivative of the phase across the wall is the basis of the induction profile, integrated along the electron path [22]. The induction profiles are shown in Fig. 8 for the linear wall and here the difference for the 500 µm TIE reconstruction is marked. While the centre of the wall shows a section of nearly linear variation the slope is larger than that associated with the input phase. Furthermore the extremities of the wall are considerably rounded indicating a loss of the high spatial frequency components in the profile. However, the same reconstructions from a hyperbolic tangent or arctangent function with the same width parameter show excellent reconstruction even at the 500 µm defocus. This is not so surprising when looking at Fig. 6. Of course, the phase gradient profiles of these trigonometric functions do not have the significant high spatial frequency components that are present in the linear wall.

5. Conclusions

The conditions for quantitative Lorentz TEM have been established and analysed to aid interpretation of images taken in this mode. It is apparent that great care must be taken if truly quantitative results are to be obtained either in the Fresnel images themselves or in reconstructed phase data

Detailed analysis of the formation of Fresnel images of magnetic thin films has shown that linear imaging can be achieved. Under these conditions the Fresnel images reveal the Laplacian of the sample phase function which can be directly related to the magnetisation curl component in the direction of the electron beam i.e. the Ampérian current density component in the same direction. Image simulation has allowed us to explore the linear and non-linear regime of the Fresnel mode with domain walls being used as examples. Although the linetraces from the Fresnel images show visible differences when moving into the non-linear range, this would not necessarily be apparent from a visual inspection of a grey scale image. We note that the linear domain wall showed up the most marked differences when moving outside the linear limit. The difference in images of walls described by trigonometric functions is much less apparent even over a large range of defocus. At large defocus all walls of the same width will appear to have a similar form, e.g. the profiles of the $\delta = 20 \,\mu m$ linear and arctangent walls at 500 µm defocus appear almost the same (Fig. 2). This is even more apparent if one considers the TIE reconstructed phase or phase gradient for such walls. It is important that any image or reconstructed data displayed has a clear indication of the defocus and spatial extent with which it is taken with respect to the resolution that is being sought.

As a final brief example we show some simulations from the OOMMF package of a 20-nm-thick film permalloy (Ni₈₀Fe₂₀) element with in-plane dimensions $1000 \,\mathrm{nm} \times 2000 \,\mathrm{nm}$. The cell size used for the calculation was $5 \text{ nm} \times 5 \text{ nm} \times 20 \text{ nm}$ and the ground state of the element has a four domain flux closure structure with 90° and 180° domain walls present. The out of plane Ampérian current distribution is shown in Fig. 9(a). The question arises as to what we might decide for the magnetic resolution in order to determine the defocus value. In this case a number of arguments can be made. For example the domain size is of the order of 500 nm whereas the widths of the 90° and 180° domain walls are approximately 80 and 40 nm, respectively. Additionally we have a sharp magnetic transition at the edges of the element which could be taken as 5 or 10 nm. Using the limit of linear imaging for a 200 kV microscope we could initially decide on defocus limits of 5 µm for 10 nm resolution, 100 µm for 50 nm resolution and 10 mm for 500 nm resolution. This can be

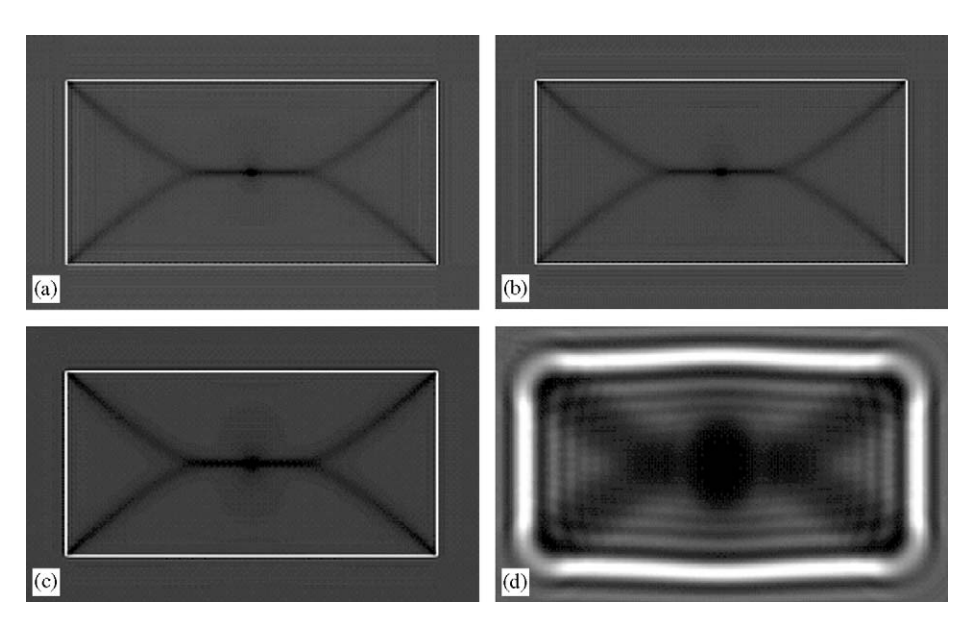


Fig. 9. (a) Out of plane magnetisation curl component for OOMMF simulated 20-nm-thick magnetic element with dimensions $1000 \text{ nm} \times 200 \text{ nm}$. (b)–(d) Calculated Fresnel TEM images for the same element at defocus values of 5, $100 \text{ and } 10000 \,\mu\text{m}$.

compared to a similar definition given when considering magnetic objects as phase gratings [10].

The images corresponding to these defocus values are shown in Figs. 9(b)–(d). Note that the contrast limits have been set to show the range of values in an individual image and not between images. Our first visual impression is that the 5 and 100 µm defocus values look like an excellent representation of the curl although the latter does appear to have wider walls and edges than that associated with the curl. By contrast the large 10 mm defocus has distorted the structure drastically. Bearing in mind the results from the previous sections and the smooth form of the domain walls expected in this type of sample we would expect the 5 and 100 µm defocus images to give reasonably quantitative results of the magnetic structure for this element although the structure at the edges of the sample where there is a discontinuity in the phase gradient will be worst affected. However, if the walls were linear then there would not be as good agreement as detailed in the previous sections particularly for the 100 µm defocus image. Also the level of contrast is very different in these two images. Looking at the signal visibility of the 180° wall section we find this is about 0.2% at the 5 μ m defocus and 4% in the 100 μ m defocus image. From a practical point of view the lower value of defocus would present problems with signal to noise ratio especially if there are non-magnetic contributions to the image contrast.

The largest defocus value (10 mm) appears very far from the linear range from the viewpoint of linearly imaging the Ampérian current density. This again highlights the care that needs to be taken for imaging the Fresnel images. In a recent paper [10] consideration was given to magnetic domain structures as phase gratings and for a sinusoidal magnetisation variation with domain size of 500 nm a defocus value of 20 mm was quoted. In that case we clearly

have a single spatial frequency component of magnetisation and therefore it is expected that this will be less sensitive to variations in the transfer function with defocus than domains which are more uniform in magnetisation. In the former the Ampérian current density varies slowly over the length of the domain while in the latter the Ampérian current density is low within the domain and restricted to the edge of close to the domain boundary i.e. spatial frequencies corresponding to the edge and domain wall width.

In the extreme case we could compare a sinusoidal magnetisation variation with a square wave pattern both having the same period. The phase associated with these would be a sinusoid and a triangular wave, respectively. Additionally, the Laplacian of these functions are sinusoid for the former and for the square wave a function that is zero everywhere except at the boundaries where there would be spikes of alternate polarity. Linear Fresnel images would be expected to have the form of the Laplacian. As can be seen (Fig. 9(d)) using the domain size as a guide for the defocus results in an image which does not reflect the Ampérian current density. At the tens of mm defocus values the sinusoid and square wave magnetisation patterns would give very similar Fresnel images as the high spatial frequency components in the latter would be smoothed out at this defocus. This emphasises the point made in Figs. 5–8 regarding the loss of high spatial frequency information with increasing defocus, in particular the forms of the intensity profiles for the different walls at large defocus. In short, the spatial frequencies associated with the Ampérian current density is really a better guide for determining the defocus value.

A good idea would be to compare a Fresnel image sequence with variable defocus through and beyond the linear regime. Clearly, the visibility of the signal is crucial in determining the viability of the technique. In this respect, the important parameters are sample magnetisation and thickness together with required resolution and therefore the associated defocus for linear imaging. We are currently working on testing the outcomes of the results given in this paper on experimental data for future publication.

The work in this paper has only been concerned with interpretation of the magnetic phase contribution to Fresnel imaging i.e. Lorentz TEM. In reality, most samples will additionally have amplitude and non-magnetic phase contributions and these will create problems in interpreting the magnetic part of the contrast. Already, recent work has been carried out to separate the magnetic and electrostatic phase contributions from experimental images by taking sets of images at different accelerating voltages [21]. However, the TIE imaging method presents considerable challenges if it is to compete with established TEM methods such as electron holography and differential phase contrast [18]. Current experimental results in conjunction with theoretical work and simulations indicate that this is well worth pursuing.

Acknowledgements

We appreciate helpful discussions with Dr. Shakul Tandon during a visit to our laboratory. In addition, we are grateful to the Nuffield Foundation and the Engineering and Physical Sciences Research council for funding which allowed this project to be undertaken.

References

- [1] M.E. Hale, H.W. Fuller, H Rubenstein, J. Appl. Phys. 30 (1959) 789.
- [2] H. Gong, J.N. Chapman, J. Magn. Magn. Mater. 67 (1987) 4.
- [3] S.J. Lloyd, N.D. Mathur, J.C. Loudon, P.A. Midgley, Phys. Rev. B 64 (2001) 172407.
- [4] D. Paganin, K.A. Nugent, Phys. Rev. Lett. 80 (1998) 2586.
- [5] S. Bajt, A. Barty, K.A. Nugent, M. McCartney, M. Wall, D. Paganin, Ultramicroscopy 83 (2000) 67.
- [6] M. De Graef, Y. Zhu, J. Appl. Phys. 89 (2001) 7177.
- [7] J.M. Cowley, Diffraction Physics, 2nd Edition, North Holland, Amsterdam, 1975.
- [8] J.H.C. Spence, Experimental High Resolution Electron Microscopy, 2nd Edition, Oxford University Press, New York, 1988.
- [9] R.E. Dunin-Borkowski, Ultramicroscopy 83 (2000) 193.
- [10] M. Beleggia, M.A. Schofield, V.V. Volkov, Y. Zhu, Ultramicroscopy 102 (2004) 37.
- [11] P. Donnadieu, M. Verdier, G. Berthomé, P. Mur, Ultramicroscopy 100 (2004) 79.
- [12] S. McVitie, G.S. White, J. Phys. D 37 (2004) 280.
- [13] Y. Aharonov, D. Bohm, Phys. Rev. 115 (1959) 485.
- [14] I.A. Beardsley, IEEE Trans. Magn. 25 (1989) 671.
- [15] V.V. Volkov, Y. Zhu, M. De Graef, Micron 33 (2002) 411.
- [16] T.E. Gureyev, K.A. Nugent, J. Opt. Soc. Am. A 13 (1996) 1670.
- [17] M. Mansuripur, J. Appl. Phys. 69 (1991) 24554.
- [18] S. McVitie, G.S. White, J. Scott, P. Warin, J.N. Chapman, J. Appl. Phys. 90 (2001) 5220.
- [19] M.J. Donahue, D.G. Porter, NISTIR 6376, National Institute of Standards and Technology, 100 Bureau Drive, Gaithersburg, MD, USA, 1999; the current URL: http://math.nist.gov/oommf/
- [20] C.J. García-Cervera, Eur. J. Appl. Math. 15 (2004) 451.
- [21] A. Kohn, A.K. Petford-Long, T.C. Anthony, Phys. Rev. B 72 (2005) 014444.
- [22] J.N. Chapman, M.R. Scheinfein, J. Magn. Magn. Mater. 200 (1999) 729.